# Stochastic Resonance in Chemistry. 2. The Peroxidase−Oxidase Reaction

**A. Förster, M. Merget, and F. W. Schneider***

*Institute of Physical Chemistry, University of Würzburg, Marcusstrasse 9-11, D-97070 Würzburg, Germany*

*Received: August 4, 1995; In Final Form: October 11, 1995*[⊗]

We show that the phenomenon of stochastic resonance exists in the enzymatic peroxidase−oxidase reaction. The free-running system is placed in an excitable steady state close to a supercritical Hopf bifurcation. When a sinusoidal flow rate signal and increasing noise are imposed on this focal steady state and a threshold is crossed, the system responds with the generation of bursts. When stochastic resonance is achieved, the interspike histogram and the plot of the signal-to-noise ratio pass through a maximum at an optimal noise level. We compare the experimental results with calculations of the Hung−Schreiber−Ross model.

## 1. Introduction

In concurrent work (part 1 of this series) we have demonstrated the occurrence of stochastic resonance (SR) in a nonlinear chemical reaction, namely, the Belousov−Zhabothinsky (BZ) reaction.[1] Stochastic resonance is a term given to the enhancement of a weak periodic signal by noise in a system with a threshold. When the threshold is crossed by the sum of the amplitudes of the subthreshold periodic signal and of the noise, a response signal is produced in the form of a burst.[2−5] For multiple crossings of the threshold, a time series of bursts is obtained, which is analyzed in the form either of an interspike histogram or by the signal-to-noise ratios (S/N) of the respective Fourier spectra. It is then found that an optimal noise level exists for the detection of the periodic signal. Stochastic resonance can occur in physical,[6−13] and biological systems[14,15] as described in a recent review article.[2] In the present study we investigate the enzymatic peroxidase−oxidase (PO)[16−21] reaction in a focal (excitable) steady state.[21] Sinusoidal or random perturbations of focal steady states have been applied previously to obtain the resonance frequency of a focus.[22−25] The threshold of a chemical nonlinear system is a complex function of several parameters among which are the distance of the focus from the nearby Hopf bifurcation and the frequency of the external sinusoidal signal. In the PO reaction the threshold is represented by a primary Hopf bifurcation leading to small sinusoidal P1* oscillations and a subsequent secondary Hopf bifurcation leading to mixed-mode oscillations with large amplitudes. Exitation of the focus into the latter large-amplitude oscillations produces the bursts. This secondary Hopf bifurcation is also called a torus bifurcation.[20] The periodic signal and the noise are imposed on the inflow of $O_2$ into the reactor.

## 2. Experimental Setup

**Materials.** Peroxidase from horseradish (HRP, RZ 3.05, activity 270 units/mg of solid) was purchased from Sigma as a salt-free powder. Glucose-6-phosphate dehydrogenase (DH) from leuconostic mesenteroides (540 units of $\beta$-$NAD^+$/mg of protein) was purchased from Sigma as a biuret suspension. $\beta$-$NAD^+$ from yeast (99%) of D-glucose-6-phosphate disodium salt (G6P, 99%) were purchased from Sigma. 2,4-Dichlorophenol (DCP) and methylene blue (MB) were purchased from Aldrich.

*CSTR (Continuous Flow Stirred Tank Reactor).* A Plexiglas CSTR of 4.7 mL liquid volume is used (Figure 1).[20] The gas volume above the liquid volume is 2.0 mL. An unsymmetric magnetic stirrer of about 1.5 mL self-volume is driven by a small motor. The solution is stirred, and therefore the oxygen inflow is limited by mass transport.[26] The oxygen mass transport into the reactor is a sensitive bifurcation parameter and dependent on the stirring rate. Therefore all experiments were done at a constant stirring rate of 750 rpm. The average $O_2$ concentration of the gaseous mixture, the total gas flow rate, the solution volume, the liquid surface area, and the temperature are kept constant in our experiments.

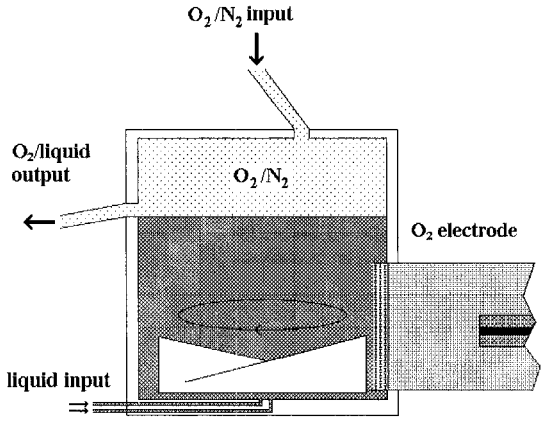


**Figure 1.** CSTR (4.7 mL volume) with two inlets for the reactant solutions, gas inlet, gas/liquid outlet, and $O_2$ electrode. Quartz glass windows are parallel to the paper plane. Plexiglas sides and UV−vis light beam are perpendicular to the plane. The $O_2$ flow rate is modulated sinusoidally and by stochastic noise.

**Preparation of Inflow Components.** All reactants were dissolved in aqueous 0.1 M phosphate buffer (pH 5.8) containing 1 $\mu$M MB and 50 $\mu$M DCP. All solutions were prepared in an argon atmosphere before each measurement. We used two gas-tight syringes (Hamilton) filled with $NAD^+$/G6P solution and DH/HRP solution with the following concentrations:

$$\text{syringe 1:} \quad [\text{HRP}] = 150 \text{ units/mL}, [\text{DH}] = 5 \text{ units/mL}$$

$$\text{syringe 2:} \quad [\text{NAD}^+] = 3.0 \text{ mM}, [\text{G6P}] = 50 \text{ mM}$$

To obtain reactor concentrations, divide by 2. All experiments were done at pH 5.60.

**Continuous Flow Conditions.** A self-designed high-precision syringe pump driven by a computer-linked stepping motor was employed to control the flow rate of the reactants into the CSTR. The stepping frequency was 8 Hz in all experiments producing a practically constant flow rate at $k_{f(\text{liquid})} = 1.35 \times$

* To whom correspondence should be addressed.
[⊗] Abstract published in *Advance ACS Abstracts,* February 15, 1996.

0022-3654/96/20100-4442$12.00/0 

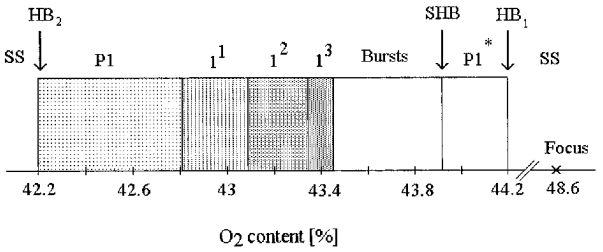


**Figure 2.** Bifurcation diagram for the free-running PO reaction with the parameters given in the text. P1 marks a region of regular period-1 oscillations. The $1^1$, $1^2$, and $1^3$ states are Farey ordered mixed-mode patterns.[20] The secondary Hopf bifurcation (SHB) is located at an $O_2$ content of 43.9%. The focus ($O_2$ content of 48.6%) is located 10% above the supercritical Hopf bifurcation ($HB_1$ at $O_2$ content of 44.2%).

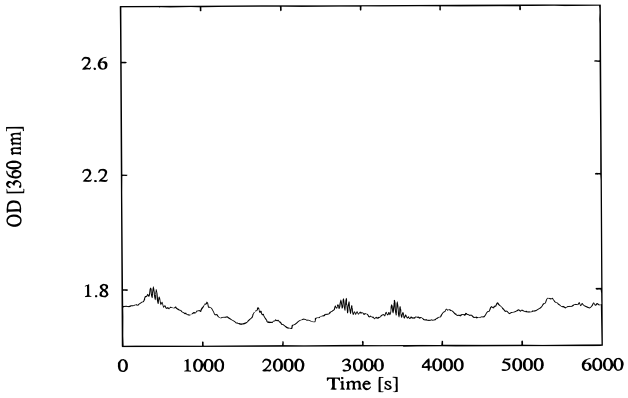


**Figure 3.** NADH absorption [360 nm] versus time at a noise amplitude $\beta = 0$.

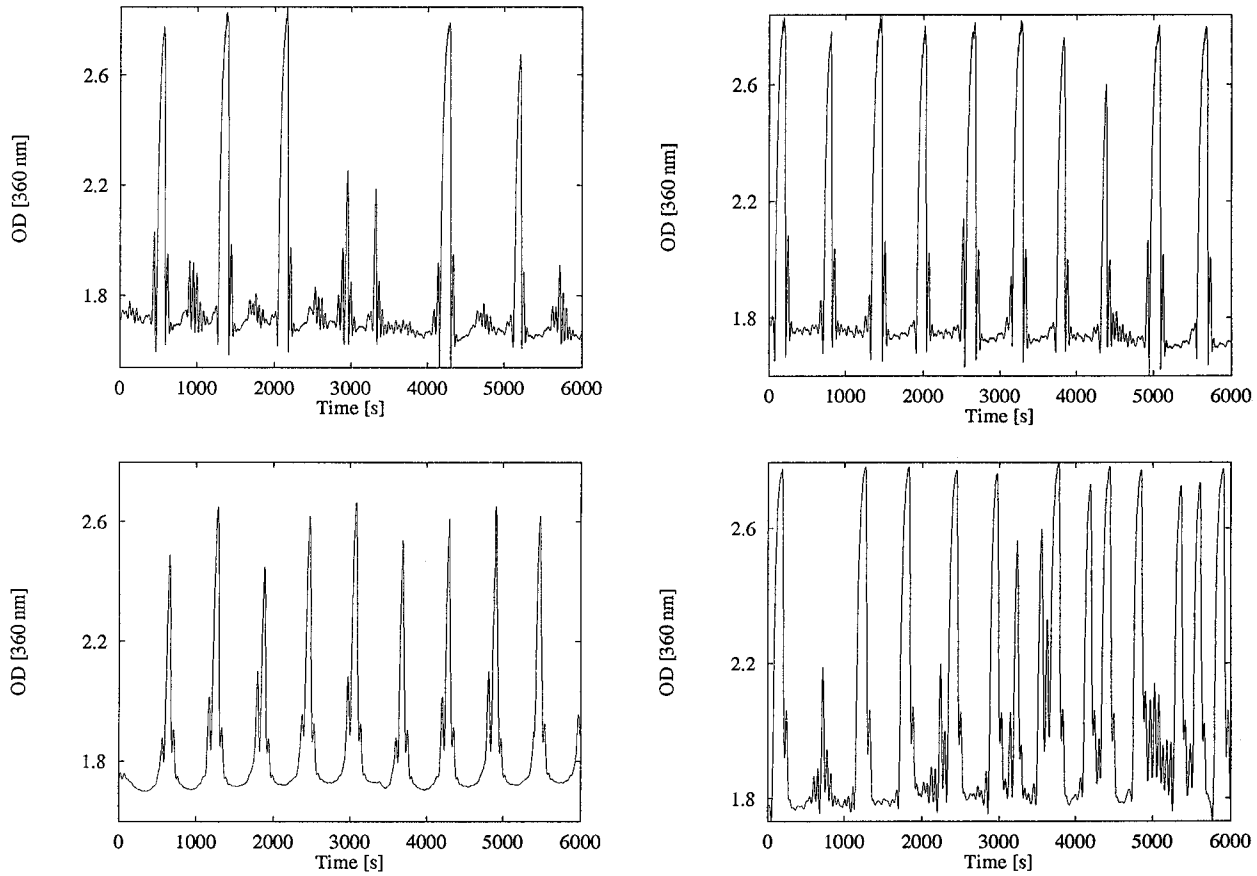


**Figure 4.** For the data evaluation of the interspike histograms only those bursts are used whose absorption was larger than 2.4. (a, top left) NADH absorption [360 nm] versus time at $\beta = 0.04$. (b, top right) NADH absorption [360 nm] versus time at $\beta = 0.06$. (c, bottom left) NADH absorption [360 nm] versus time at $\beta = 0.08$. (d, bottom right) NADH absorption [360 nm] versus time at $\beta = 0.16$.

$10^{-2}$ min$^{-1}$ (residence time $\tau = 74$ min). The average flow rate of the gaseous mixture $O_2/N_2$ was constant at $k°_{f(gas)} = 0.6$ mL/s in all experiments. In the experimental bifurcation diagram (Figure 2) the $O_2$ content in the $O_2/N_2$ mixture is the bifurcation parameter. The $O_2$ content at the Hopf bifurcation $HB_1$ was determined to be $[O_2]_{Hopf} = 44.2\%$. Here the oscillations give way to a stable focus. When the $O_2$ content in the gas mixture is decreased a small region of sinusoidal P1* oscillations of high frequency and low amplitude appear. A further reduction of $O_2$ leads to the appearance of large amplitude oscillations called bursts. The bursts start at a secondary Hopf bifurcation (SHR).[20] The average $O_2$ flow rate at the applied focus is ≈10% above the primary Hopf bifurcation.

**Temperature.** The syringes containing the input chemicals, the tubing, and the reactor were thermostated at 25 °C for all experiments.

**Detection.** The time series of NADH absorption (360 nm detection wavelength) and compound III (418 nm) were measured with a diode array spectrophotometer (Hewlett-Packard 8452A) with a sampling rate of 1 Hz. The time series of the oxygen potential were measured with an oxygen-selective Clark electrode and a microprocessor oximeter (WTW Oxi 96) with a sampling rate of 1 Hz. In the experiments the stochastic resonance is measured by the probability distribution of the time intervals between the bursts, the so-called interspike histogram. The width of the bars in the histogram is chosen to be 10 s for optimal results. We also calculated the signal-to-noise ratio (S/N) from the Fourier spectra as the ratio of the fundamental peak to the background noise at the frequency of the sinusoidal signal. For the calculation of the interspike histograms and the Fourier spectra we used 12 000 data points corresponding to time series of 12 000 s.

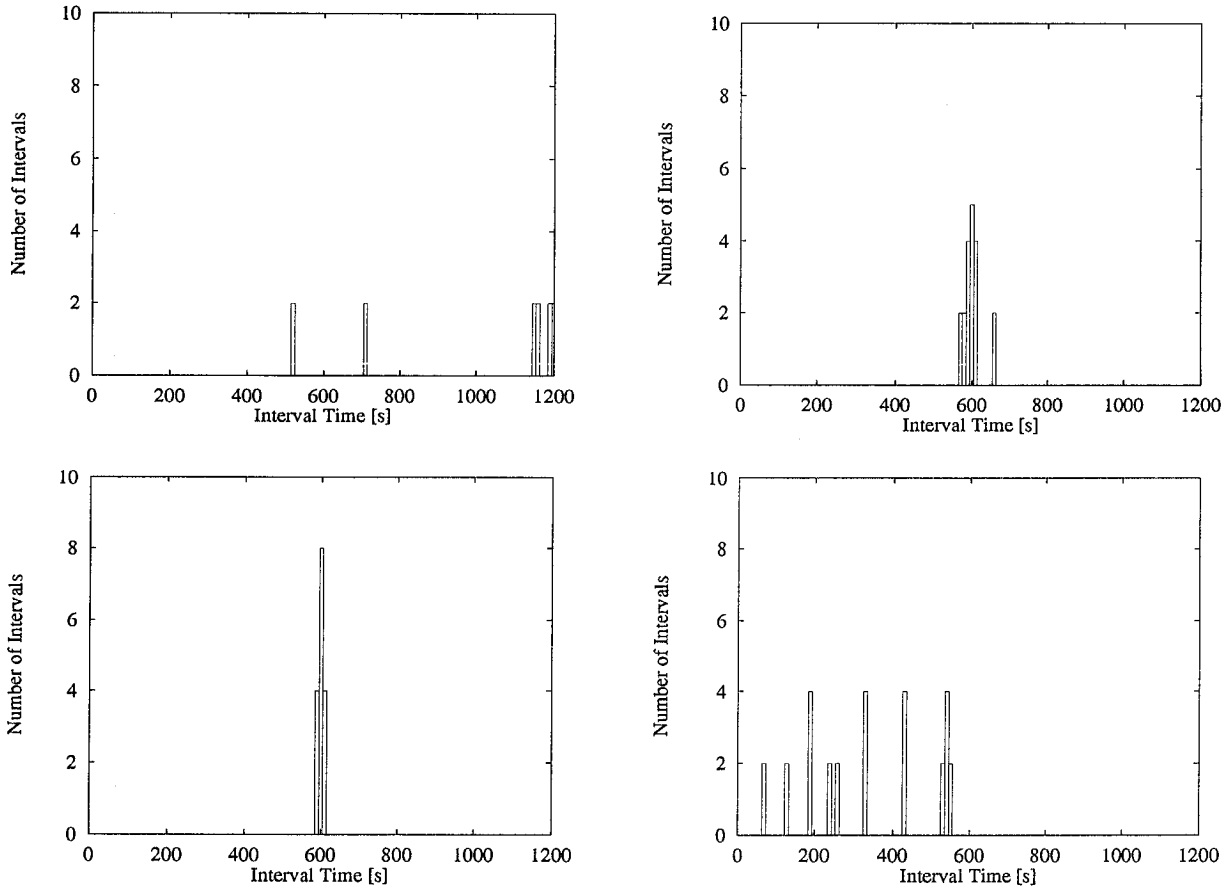


**Figure 5.** (a, top left) Interspike histogram of the time series at $\beta = 0.04$. (b, top right) Interspike histogram of the time series at $\beta = 0.06$. (c, bottom left) Interspike histogram of the time series at $\beta = 0.08$. (d, bottom right) Interspike histogram of the time series at $\beta = 0.16$.

**Periodic and Stochastic Modulation of the $O_2$-Flow Rate.** Two computer-linked mass flow controllers (MKS type 1259C) for $O_2$ and $N_2$, respectively, were employed to mix and regulate the gas flow and $O_2$ content at atmospheric pressure. During the perturbation experiments the liquid flow rates through the reactor remained constant. The imposed sinusoidal and stochastic modulation were calculated by a computer.

We imposed a sinusoidal function of amplitude $\alpha$ and frequency $\omega$ together with noise of amplitude $\beta$ and pulse length $\delta$ on the $O_2$ flow rate according to eq 1, where $k_f^\circ(O_2)$ is the

$$k_f(O_2) = k_f^\circ(O_2)(1 + \alpha \sin(\omega t) + \beta R(\delta)) \qquad (1)$$

constant $O_2$ flow rate at the focus ($=k^\circ_{f(gas)} \times$ ($O_2$ content)). The noise $R(\delta)$ is generated on a computer by a random number generator. The amplitude of the sinusoidal $O_2$ flow rate is kept constant at $\alpha = 0.19$. The frequency of the sinusoidal signal is $\omega = 0.011$ rad/s, corresponding to an input period of $T = 600$ s. The variations in the noise amplitudes were chosen to be statistical according to a Gaussian distribution with $0 < \beta < 0.16$. The stochastic noise amplitudes were imposed at intervals of 10 s (0.628 rad/s), which is about 60 times smaller than the imposed periodic signal and 10 times smaller than the natural period of the focus.

## 3. Results

**3.1. Experimental Results.** A focus (focal steady state) was established in the CSTR at a constant flow rate $k_{f(liquid)} = 1.35\ 10^{-2}\ s^{-1}$ (residence time $\tau = 74$ min) and an oxygen content of 48.6% (Figure 2) at a constant gas flow. The focus was located about 10% above the supercritical Hopf bifurcation (Figure 2). When a sinusoidal variation of the $O_2$ flow rate ($\alpha = 0.19$, $T =$ 600 s) is imposed on the focus without added noise, the focus responds without bursting showing sinusoidal oscillations of period $T_{out} = 600$ s at low amplitudes as detected by the absorption of NADH at 360 nm (Figure 3) or by the $O_2$ electrode, whose phase is slightly shifted with respect to the NADH oscillations. The response signal (NADH concentration) also shows small damped P1* oscillations superimposed on the oscillations with $T = 600$ s. Bursting does not occur under these conditions, because the system has not yet crossed the threshold despite the presence of an estimated natural noise level of $\leq$2%. When noise of amplitude $\beta = 0.04$ at pulse length $\delta = 10$ s is added to the sinusoidal $O_2$ signal, the focus responds with irregular bursting (Figure 4a). However, burst intervals corresponding to the period of the sinusoidal signal ($T = 600$ s, $\omega = 0.011$ rad/s) are not observed at $T_{out} = 600$ s in the case of $\beta = 0.04$ as seen from the interspike (or interburst) histogram (Figure 5a), where $T_{out}$ is the response period. Likewise, the Fourier spectrum is broad and does not show any strong features (Figure 6a). When the noise amplitude is increased bursting becomes more regular. At a noise amplitude of $\beta = 0.06$ an almost regular bursting behavior is observed (Figure 4b), whose histogram shows five events (bursts) at $T_{out} = 600$ s (Figure 5b). The Fourier spectrum shows a S/N ratio of about 6 at $T_{out} = 600$ s (Figure 6b). It is seen that a given burst may be accompanied by several smaller satellite bursts below OD = 2.4 (Figure 4) which are not counted. At a noise amplitude of $\beta = 0.08$ an optimal amplification of the sinusoidal signal is observed (Figure 4c). Now all bursts appear in a burst interval between 585 and 615 s around $T_{out} = 600$ s (Figure 5c). The S/N ratio at the signal frequency is relatively high (S/N $\approx$ 23, Figure 6c). Figure 4d shows a time series at a still higher noise amplitude of $\beta = 0.16$. Here the noise is sufficiently large to

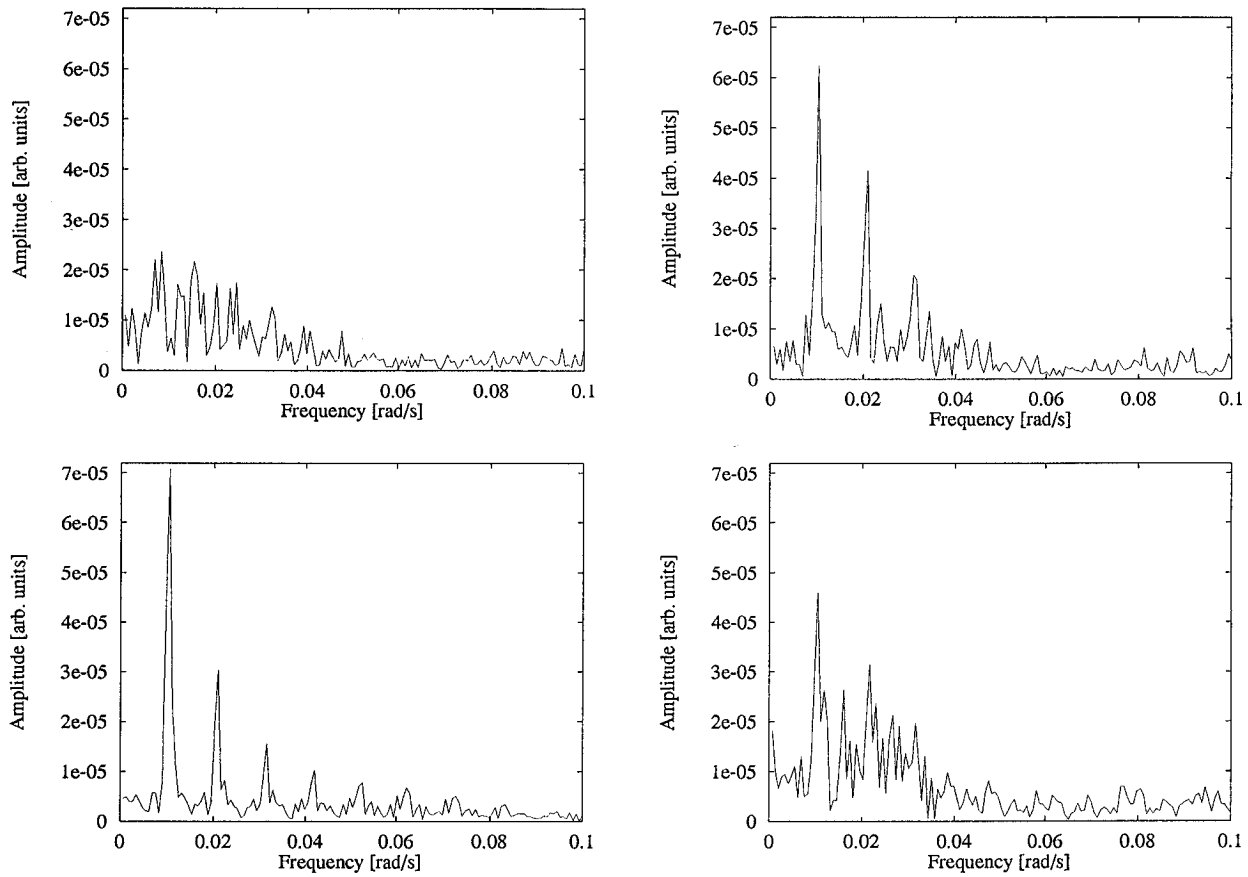


**Figure 6.** (a, top left) Fourier spectrum of the time series at $\beta = 0.04$. (b, top right) Fourier spectrum of the time series at $\beta = 0.06$. (c, bottom left) Fourier spectrum of the time series at $\beta = 0.08$. (d, bottom right) Fourier spectrum of the time series at $\beta = 0.16$.

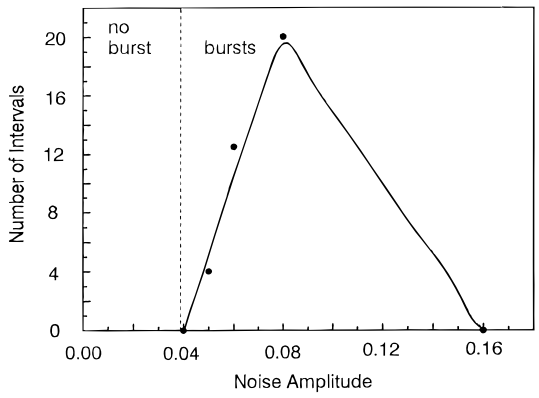


**Figure 7.** Number of bursts occurring in the interval from 595 to 605 s versus the maximal noise amplitude. It is located at $\beta \approx 0.075$.

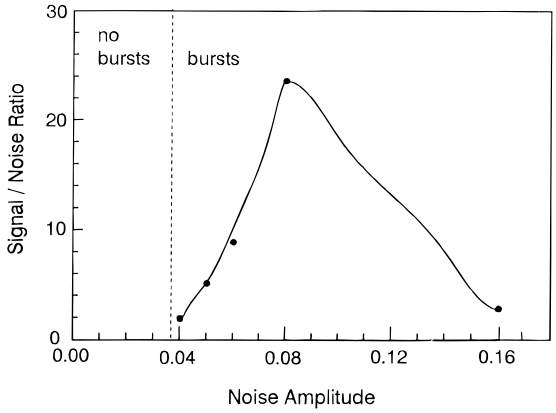


**Figure 8.** Experimental signal-to-noise ratio evaluated from the Fourier spectra versus the maximal noise amplitude. The maximum is located at $\beta \approx 0.077$.

cause multiple bursts per oscillation. The histogram shows a broad distribution of burst intervals without any bursts at $T_{out} = 600$ s (Figure 5d). The Fourier spectrum shows a low S/N peak at the periodic signal ($T = 600$ s), and the background noise is relatively high (Figure 6d). In all experiments with a periodic signal of $T = 600$ s burst intervals smaller than 90 s were not observed. Thus we assume that the refractory time of the system is about 90 s.

When the number of bursts in the time interval between 595 and 605 s is plotted versus the noise amplitude, a maximum in the curve is obtained at $\beta \approx 0.075$ (Figure 7). This maximum denotes the optimal noise level for the detection of the sinusoidal $O_2$ input signal at $T = 600$ s and $\alpha = 0.19$. The plot of the S/N ratios from the Fourier spectra versus the noise amplitude (Figure 8) shows a maximum at practically the same noise amplitude ($\beta \approx 0.077$) as in the case of the interspike histograms (Figure 7).

We also investigated a signal of a smaller period ($T = 400$ s) at the same amplitude ($\alpha = 0.19$), where the maximum response occured at a higher value of the noise amplitude, namely, $\beta = 0.12$ (not shown). Thus the optimal noise level depends among other things on the frequency of the signal to be detected.

**3.2. Model Calculations.** *Hung−Schreiber−Ross Model.* In the following we use the Hung−Schreiber−Ross (HSR)[27] model which represents an extension of the Aguda−Larter model.[28] The HSR model consists of 12 variables and 18 steps. All rate constants and starting concentrations used to obtain a focus are given in Table 1. The employed focus is located 1.4% above the Hopf bifurcation HB (Figure 9). In contrast to the experimental PO system, a region of low-amplitude P1* oscillations have not been found in the model calculations. All

**TABLE 1: Values of the Parameters and Initial Conditions of the Variables Used in the Hung−Schreiber−Ross Model Calculations**

| The HSR Model | |
|---|---|
| $Per^{3+} + H_2O_2 \rightarrow CoI$ | $k_1 = 4.0 \times 10^7\ M^{-1}\ s^{-1}$ |
| $CoI + NADH \rightarrow CoII + NAD^{\bullet}$ | $k_2 = 5.0 \times 10^5\ M^{-1}\ s^{-1}$ |
| $CoII + NADH \rightarrow Per^{3+} + NAD^{\bullet}$ | $k_3 = 1.0 \times 10^6\ M^{-1}\ s^{-1}$ |
| $Per^{3+} + NAD^{\bullet} \rightarrow Per^{2+} + NAD^{+}$ | $k_4 = 1.0 \times 10^6\ M^{-1}\ s^{-1}$ |
| $Per^{2+} + O_2 \rightarrow CoIII$ | $k_5 = 2.0 \times 10^7\ M^{-1}\ s^{-1}$ |
| $CoIII + NAD^{\bullet} + H^{+} \rightarrow CoI + NAD^{+}$ | $k_6 = 3.0 \times 10^8\ M^{-1}\ s^{-1}$ |
| $Per^{3+} + O_2^{\bullet} \rightarrow CoIII$ | $k_7 = 3.0 \times 10^7\ M^{-1}\ s^{-1}$ |
| $NAD^{\bullet} + O_2 \rightarrow NAD^{+} + O_2^{\bullet -}$ | $k_8 = 2.0 \times 10^8\ M^{-1}\ s^{-1}$ |
| $O_2^{\bullet} + NADH + H^{+} \rightarrow H_2O_2 + NAD^{\bullet}$ | $k_9 = 3.0 \times 10^5\ M^{-1}\ s^{-1}$ |
| $2NAD^{\bullet} \rightarrow (NAD)_2$ | $k_{10} = 1.0 \times 10^8\ M^{-1}\ s^{-1}$ |
| $2O_2^{\bullet -} + 2H^{+} \rightarrow H_2O_2 + O_2$ | $k_{11} = 2.0 \times 10^7\ M^{-1}\ s^{-1}$ |
| $NADH + O_2 + H^{+} \rightarrow H_2O_2 + NAD^{+}$ | $k_{12} = 5.0 \times 10^{-5}\ M^{-1}\ s^{-1}$ |
| $NADH_0 \rightarrow NADH$ | $k_{13} = 1.52 \times 10^7\ M^{-1}\ s^{-1}$ |
| $O_2(g) \rightarrow O_2(aq)$ | $k_{14}$ = bifurcation parameter |
| $O_2(aq) \rightarrow O_2(g)$ | $k_{15} = 5.0 \times 10^{-3}\ s^{-1}$ |
| $NADH + H_2O_2 + H^{+} \rightarrow 2H_2O + NAD^{+}$ | $k_{16} = 1.0 \times 10^7\ M^{-1}\ s^{-1}$ |
| $CoIII + DCP \rightarrow Per^{2+} + O_2^{\bullet -} + DCP^{\bullet}$ | $k_{17} = 1.0 \times 10^3\ M^{-1}\ s^{-1}$ |
| $DCP^{\bullet} + NADH \rightarrow DCP + NAD^{\bullet}$ | $k_{18} = 1.0 \times 10^1\ M^{-1}\ s^{-1}$ |
| flow rate: $k_{14} = k_{f(O2)} = 7.4935 \times 10^{-8}\ M\ s^{-1}$ | |

| Initial Values of the Variables |
|---|
| $[coI] + [coII] + [coIII] + [Per^{2+}] + [Per^{3+}] = 2.7 \times 10^{-6}$ mol/L |
| $[Per^{3+}] = 1.5 \times 10^{-6}$ mol/L |
| $[Per^{2+}] = [coI] = [coII] = [coIII] = 0.0$ mol/L |
| $[H_2O_2] = 1.0 \times 10^{-10}$ mol/L |
| $[NADH] = 2.09 \times 10^{-6}$ mol/L |
| $[NAD_0] = [NAD^{+}] = [O_2^{\bullet -}] = 0.0$ mol/L |
| $[O_2] = 0.758 \times 10^{-6}$ mol/L |
| $[DCP] = 3.7 \times 10^{-5}$ mol/L |

integrations were done using the Gear algorithm.[29,30] Two terms, representing the sinusoidal signal and Gaussian distributed noise are added to the reaction rate $k_{14}°$ according to eq 2. In

$$k_{14} = k_{14}°(1 + \alpha \sin(\omega t) + \beta R(\delta)) \qquad (2)$$

the case of the model simulations $k_{14}$ is a convenient bifurcation parameter. It describes the mass transport of $O_2$ from the gas phase into the liquid, where $k_{14}°$ refers to the constant $O_2$ flow rate at the focus. The amplitude $\alpha$ of the sinusoidal signal is set to 0.70. An identical sinusoidal signal frequency ($\omega = 0.011$ rad/s, $T = 600$ s) as in the experiments is chosen. $\beta$ is varied between 0 and 0.28 for a noise pulse length of $\delta = 10$ s. In the model calculations stochastic resonance is demonstrated by the interspike histogram (Figure 10) and by the signal-to-noise ratio (S/N, Figure 11) which is determined from the Fourier spectra in a similar fashion as in the experiments. We used 200 000 points calculated at intervals of 1 s. The first $1 \times 10^6$ s were omitted due to transient behavior.

*Numerical Results.* A sinusoidal signal frequency of $\omega = 0.011$ rad/s ($T = 600$ s) with an amplitude of $\alpha = 0.70$ is imposed on the focus. Under these constraints sinusoidal response oscillations with low amplitudes and an identical period of $T_{out} = 600$ s emerge. If a certain noise level is applied in addition to the sinusoidal signal, bursting occurs when the threshold is crossed. Figure 10 shows the number of bursts in the interval between 595 and 605 s around $T_{out} = 600$ s. A maximum is observed at a noise level of $\beta \approx 0.056$. We evaluated the signal-to-noise ratio at different noise levels from the Fourier spectra as the ratio of the fundamental peak to the background noise at the frequency of the sinusoidal signal (Figure 11). They show a maximum at approximately the same noise amplitude ($\beta \approx 0.058$) as in the case of the interspike histograms (Figure 10).

We further studied a larger sinusoidal signal ($\alpha = 0.90$) at the same signal frequency of $\omega = 0.011$ rad/s ($T = 600$ s).

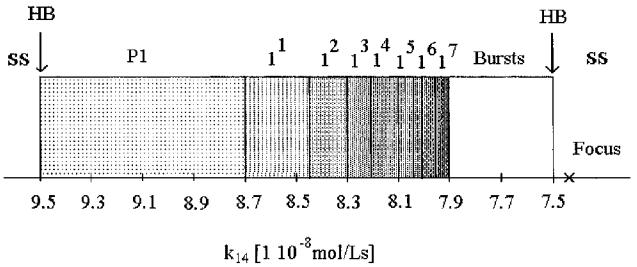


**Figure 9.** Bifurcation diagram of the free-running Hung−Schreiber−Ross (HSR) model with the parameters given in Table 1. P1 marks a region of period-1 oscillations. The $1^1$ to $1^7$ states are Farey ordered mixed-mode oscillations. The focus ($k_{14} = 7.4935$ mol/Ls) is located 1.4% above the Hopf bifurcation (HB at $k_{14} = 7.55$ mol/Ls).

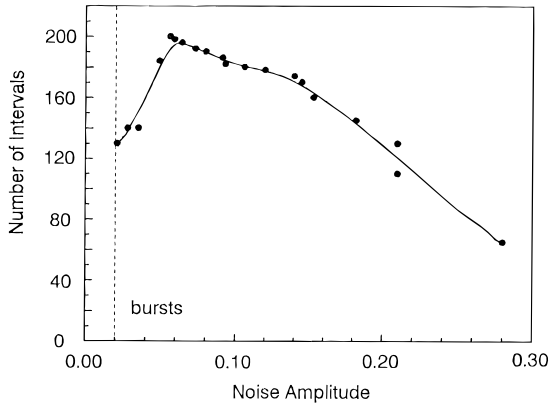


**Figure 10.** Number of bursts occuring in the interval between 595 and 605 s versus the noise amplitude in the HSR model. The maximum is located at $\beta \approx 0.056$.

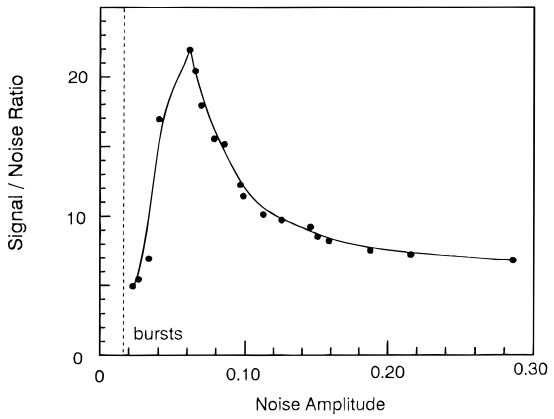


**Figure 11.** Signal-to-noise ratio evaluated from the Fourier spectra versus noise amplitude in the HSR model. The maximum is reached at about the same $\beta \approx 0.058$, as in Figure 10.

Here the maximal effect of the stochastic resonance occurs at a lower noise amplitude of $\beta \approx 0.005$ (not shown) as expected.

## 4. Discussion

We have observed the phenomenon of stochastic resonance in the nonlinear enzymatic PO reaction whose concentrations and flow rates were adjusted to display the equivalent of an excitation threshold. In the experiments the threshold is represented by a bifurcation between the focus and low-amplitude P1* oscillations followed by complex large-amplitude oscillations. In the present PO reaction as well as in other nonlinear chemical reactions,[1] the optimal noise level depends on several factors, such as the amplitude and the frequency of the sinusoidal signal, the noise pulse length, and the distance of the signal to the threshold. For high signal frequencies a

higher noise level is required to obtain stochastic resonance. This may be due to the fact that at high signal frequencies the system does not spend a sufficiently long time near the excitation threshold region. Like in the BZ reaction,[1] an upper frequency limit for the sinusoidal signal to be detected is given by the refractory time of the system (90 s). If sinusoidal input signals of shorter periods than the refractory time are applied in the HSR model, only multiples of the sinusoidal period are observed in the system's response. With increasing amplitude of the periodic signal the sum of signal and noise crosses the excitation threshold at lower optimal noise levels. The experiments were compared with calculations of the HSR model. The calculations are in qualitative agreement with the experiments. Thus stochastic resonance occurs in several chemical nonlinear reactions, namely in the present enzymatic PO reaction, in the organic/inorganic BZ reaction (part 1),[1] and in the minimal bromate oscillator (part 3).[31] Further detailed work is in progress.

**Acknowledgment.** We thank A. Guderian, G. Dechert, and K. P. W. Zeyer for valuable discussions. We further thank the Deutsche Forschungsgemeinschaft and the Fonds der Chemischen Ind. for partial support of this work.

## References and Notes

(1) Guderian, A.; Dechert, G.; Zeyer, K. P. W.; Schneider, F. W. *J. Phys. Chem.* **1996**, *100*, 4437.
(2) Wiesenfeld, K.; Moss, F. *Nature* **1995**, *373*, 33.
(3) Benzi, R.; Sutera, A.; Vulpiani, A. *J. Phys.* **1981**, *14A*, L453.
(4) Nicolis, C. *Tellus* **1982**, *34*, 1.
(5) Benzi, R.; Parisi, G.; Sutera, A.; Vulpiani, A. *Tellus* **1982**, *34*, 10.
(6) Fauve, S.; Heslot, F. *Phys. Lett.* **1983**, *97A*, 5.
(7) McNamara, B.; Wiesenfeld, K.; Roy, R. *Phys. Rev. Lett.* **1988**, *60*, 2626.
(8) Simon, A.; Libchaber, A. *Phys. Rev. Lett.* **1992**, *68*, 3375.
(9) Grammaitoni, L.; Martinelli, M.; Pardi, L.; Santucci, S. *Phys. Rev. Lett.* **1991**, *67*, 1799; *J. Statist. Phys.* **1993**, *70*, 425.
(10) Dykman, M. I.; Velikovich, A. L.; Golubev, G. P.; Luchinskii, D. G.; Tsuprikov, S. V.; *Pis'ma Zh. Eksp. Teor. Fiz.* **1991**, *53*, 182.
(11) Grohs, J.; Apanasevich, S.; Jung, P.; Issler, H.; Burak, D.; Klingshirn, C. *Phys. Rev.* **1994**, *49a*, 2199.
(12) Spano, M. L.; Wun-Fogle, M.; Ditto, W. L. *Phys. Rev.* **1992**, *46a*, 5253.
(13) Hibbs, A. D.; Singsaas, A. L.; Jacobs, E. W.; Bulsara, A. R.; Bekkedahl, J. J.; Moss, F. *J. Appl. Phys.* **1995**, *77*, 2582.
(14) Douglass, J. K.; Wilkens, L.; Pantazelou, E.; Moss, F. *Nature* **1993**, *365*, 337.
(15) Moss, F.; Douglass, J. K.; Wilkens, L.; Pierson, D.; Pantazelou, E. *Ann. N.Y. Acad. Sci.* **1993**, *706*, 26.
(16) Yamazaki, I.; Yokota, K.; Nakajama, R. *Biochem. Biophys. Res. Commun.* **1965**, *21*, 582.
(17) Nakamura, S.; Yokota, K.; Yamazaki, I. *Nature* **1969**, *222*, 794.
(18) Yamazaki, I.; Yokota, K. *Mol. Cell. Biochem.* **1973**, *2*, 39.
(19) Olsen, L. F.; Degn, H. *Biochem. Biophys. Acta* **1978**, *523*, 321.
(20) Hauck, T.; Schneider, F. W. *J. Phys. Chem.* **1993**, *97*, 391.
(21) Hauck, T.; Schneider, F. W. *J. Phys. Chem.* **1994**, *98*, 2072.
(22) Buchholtz, F.; Schneider, F. W. *J. Am. Chem. Soc.* **1983**, *105*, 7450.
(23) Münster, A. F.; Schneider, F. W. *Ber. Bunsen-Ges. Phys. Chem.* **1992**, *96*, 32.
(24) Förster, A.; Hauck, T.; Schneider, F. W. *J. Phys. Chem.* **1994**, *98*, 184.
(25) Förster, A.; Zeyer, K. P. W.; Schneider, F. W. *J. Phys. Chem.* **1995**, *99*, 11889.
(26) Olsen, D. L.; Scheeline, A. *Anal. Chim. Acta* **1993**, *283*, 703.
(27) Hung, Y.-F.; Schreiber, I.; Ross, J. *J. Phys. Chem.* **1995**, *99*, 1980.
(28) Aguda, B.; Larter, R. *J. Am. Chem. Soc.* **1991**, *113*, 7913.
(29) Gear, C. W. *Numerical Initial Value Problems in Ordinary Differential Equations*; Prentice-Hall: Englewood Cliffs, NJ, 1971; p 209.
(30) Hindmarsh, A. C. *Gear*: *Ordinary Differential Equations System Solver*; VCID 2001, rev 3, Dec 1974.
(31) Hohmann, W.; Müller, J.; Schneider, F. W. *J. Phys. Chem.*, in press.

JP952244P